Fluorinated Cyclic Ether Co-solvents for Ultra-high-Voltage Practical Lithium-Metal Batteries

Yan Zhao, Tianhong Zhou, Mario El Kazzi, and Ali Coskun*

ABSTRACT: The advancement of liquid electrolytes in Li-metal batteries is an important strategy to realize a robust and uniform solid electrolyte interphase (SEI) on the Li metal anode while simultaneously achieving high oxidative stability and addressing the shortcomings of traditional carbonate and ether-based electrolytes suffering from side reactions and high-voltage decomposition, respectively. To circumvent these challenges, here, a fluorinated dioxolane-based cyclic co-solvent, that is 2-(2,2,2-trifluoroethoxy)-4-(trifluoromethyl)-1,3-dioxolane (TTD), is developed. After pairing 1.5 M lithium bis(fluorosulfonyl)imide (LiFSI) with TTD and 1,2-dimethoxyethane (DME), the 1.5 M LiFSI-8TTD-2DME electrolyte exhibits remarkable oxidation stability up to 6 V and a Coulombic efficiency of 99.4% over 210 cycles at 3 mA cm^{-2} with a cut-off capacity of 3 mA h cm^{-2} in the Li|Cu half-cell originating from efficient regulation of the electrolyte solvation structure and consequent anion-derived inorganic SEI layer formation. Full cells with advanced electrolytes, using 20 μm of Li foil paired with the NCM811 cathode by a negative and positive capacity ratio (N/P) of 2.5, achieve 75% capacity retention after 160 cycles at 0.5 C. Furthermore, even at an ultra-high charge cut-off voltage of 4.7 V, the Li|NCM811 full cell still realizes 80% retention at 0.5 C after 100 cycles.

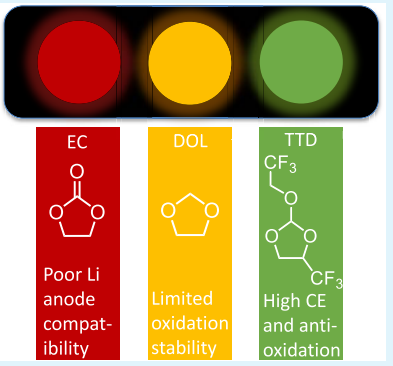

KEYWORDS: *cyclic ether, co-solvent, fluorination, electrolyte, Li-metal batteries*

INTRODUCTION

Lithium (Li)-metal batteries (LMBs) are considered as the next-generation energy storage solutions beyond Li-ion batteries (LIBs) owing to their exceptionally high energy density.[1−5] Li-metal anode (LMA) offers several advantages such as low electrochemical potential (−3.04 V) and high theoretical specific capacity (3860 mA h g^{-1}). When paired with a high-voltage nickel-rich cathode, LMBs could in principle double the attainable energy density of conventional LIBs.[6,7] However, the application of LMBs is hampered by either low thermodynamic stability of electrolytes toward LMA or their low oxidation stability. The uncontrolled reactions between the electrolyte and LMA result in a mechanically weak solid electrolyte interphase (SEI) formation on the LMA, causing continuous electrolyte consumption, low Coulombic efficiency (CE), dead Li formation, and severe capacity loss.[8,9] Therefore, achieving electrolyte compatibility through chemical structure control is crucial in high-voltage LMBs. Although commercial carbonate electrolytes can achieve a stable and robust SEI layer on the graphite anode, their low thermodynamic stability causes serious side reactions along with a porous and thick SEI layer and Li filament formation in LMBs.[10,11] Ether-based electrolytes such as 1,2-dimethoxyethane (DME) and 1,3-dioxolane (DOL), on the other hand, are widely used in Li−sulfur (Li−S) batteries owing to their Li-metal compatibility, enabling higher CE and less dendrite formation compared to carbonate electrolytes,[12] but their low anodic stability (below 4 V) at a low salt concentration (1 M) hinders their use in high-voltage LMBs.[13,14] Hence, it is rather important to develop new electrolyte chemistries to meet the requirements of both LMA and high-voltage cathodes in LMBs.

High-concentration electrolytes (HCEs) have been widely studied as solvent-in-salt electrolytes to achieve improved electrochemical stability at the expense of ionic conductivity.[15] A high salt concentration in HCEs drastically decreases free solvent molecules while promoting contact ion pairs (CIPs) and aggregate cluster formation (AGG), which improves their compatibility with both high-voltage cathodes and LMA.[13,16,17] Specifically, in HCEs, the lowest unoccupied molecular orbital (LUMO) of an anion becomes lower than that of the solvent, leading to its prior decomposition and the consequent emergence of an anion-derived and inorganic SEI layer on the LMA. Meanwhile, the decrease in the highest occupied molecular orbital (HOMO) energy of the coordinated solvent molecules enhances their oxidation stability.[18] However, the poor wettability, high cost, and viscosity of HCEs limit their

Received: April 26, 2022
Accepted: May 31, 2022
Published: June 9, 2022

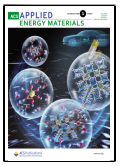

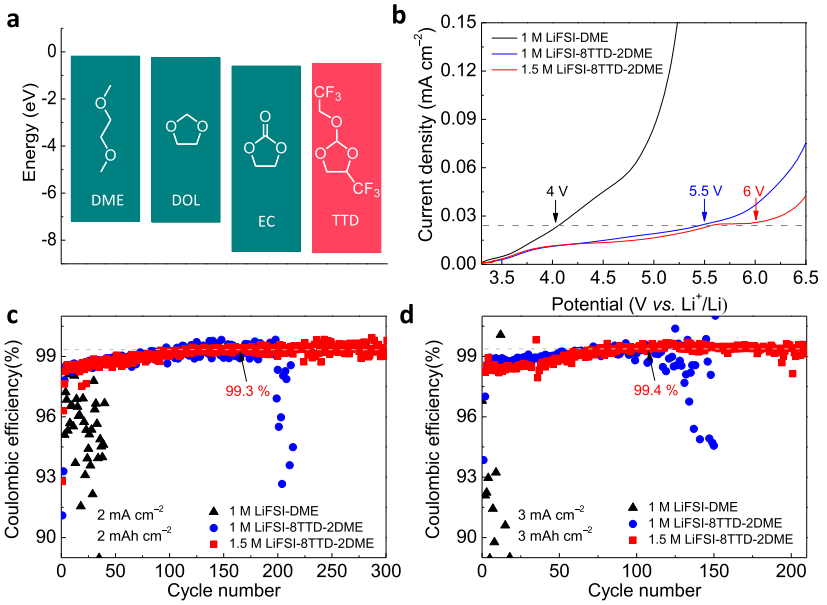

Figure 1. (a) Comparison of HOMO−LUMO energy levels of conventional solvents and TTD. (b) Analysis of electrolytes' oxidative stability using LilAl half cells tested by LSV. (c,d) Li-metal CE of LilCu cells using three different electrolytes at (c) 2 mA cm^{-2} with 2 mA h cm^{-2} capacity and (d) 3 mA cm^{-2} with 3 mA h cm^{-2} capacity.

practical application. In this direction, localized HCEs (LHCEs) were introduced to form high-concentration clusters at moderate salt concentrations by using hydrofluoroether diluents/co-solvents, that are, bis(2,2,2-trifluoroethyl) ether (BTFE),[19] 1,1,2,2-tetrafluoroethyl-2,2,3,3-tetrafluoropropylether (TTE),[20] and tris(2,2,2-trifluoroethyl)orthoformate (TFEO).[21,22] As these diluents/co-solvents can hardly solvate Li ions, they need to be paired with strongly solvating solvents, which leads to the in situ formation of high-concentration clusters between solvents and the Li salt stabilized by diluent/co-solvent molecules in LHCEs.[18,23] However, the reported LHCEs rarely exhibited ultra-high-voltage cycling such as 4.7 V for a high-nickel cathode owing to insufficient passivation. There are also recent efforts to develop solvents such as fluorinated 1,4-dimethoxylbutane (FDMB) and sulfonamide (DMTMSA) with high-voltage stability and Li^+ solvation ability through electrolyte engineering.[24,25] One common structural feature of these diluents and solvents is their linear or branched structures. Conventional carbonate or ether-based electrolytes, on the other hand, involve the mixture of cyclic and linear solvents to achieve a stable interface through their synergistic effect. Specifically, the established electrolyte in Li−S batteries, such as the DOL−DME system, exhibits high CEs and stable SEI on LMA,[12] as the ring-opening polymerization reaction of DOL enables the formation of elastomers to stabilize the LMA surface.[26,27] The low oxidation stability (<4 V) of the DOL−DME-based electrolyte, mainly derived from the high reactivity of DOL toward ring-opening polymerization,[28] however, limits its application in high-voltage LMBs, and a cyclic-linear ether mixture system with high-voltage stability has yet to be developed for LMBs. Herein, a new fluorinated cyclic dioxolane derivative, 2-(2,2,2-trifluoroethoxy)-4-(trifluoromethyl)-1,3-dioxolane (TTD), was first introduced as a co-solvent in high-voltage LMBs. The electrolyte was obtained by pairing 1.5 M lithium bis(fluorosulfonyl)imide (LiFSI) with TTD and DME in a volume ratio of 8:2 (referred to as 1.5 M LiFSI-8TTD-2DME). The electrolyte exhibited oxidation stability up to 6 V, reached a high CE value of 99.4% in a LilCu half-cell at a current density of 3 mA cm^{-2} with the capacity of 3 mA h cm^{-2}, and showed robust cycling. The wide electrochemical window and excellent LMA performance of the 1.5 M LiFSI-8TTD-2DME electrolyte enabled high-voltage LMBs, with Li foil (20 μm) being paired with the NCM811 cathode, giving the N/P ratio of 2.5, and realizing 75% capacity retention after 160 cycles. Even with an extremely high cut-off voltage of 4.7 V, the Lil NCM811 full cell still realized 80% retention after 100 cycles at 0.5 C.

RESULTS AND DISCUSSION

Cyclic solvents such as DOL and ethylene carbonate (EC) have been widely applied in conventional electrolytes. Although the severe side reaction of EC on LMA owing to the high polarity of C═O moiety causes the growth of a thick SEI layer, the low oxidation stability of DOL limits its applicability in high-voltage LMBs. In this direction, we reasoned that replacing the C═O moiety in EC with a C−O−C linker while integrating an electron-withdrawing group such as $-CF_3$ in a cyclic structure could alleviate the problems of EC and DOL by decreasing the reactivity toward LMA and extending the oxidative stability at a high voltage by lowering the HOMO energy level.[21,24,29] TTD was synthesized by the acid-catalyzed cyclization reaction of tris(2,2,2-trifluoroethyl)-orthoformate and 1,1,1-trifluoro-2,3-propanediol at 100 °C for 3 h in 58% yield. The successful synthesis of TTD was confirmed by nuclear magnetic resonance (NMR) spectroscopy analysis (Figures S1−S6).

We compared the HOMO−LUMO energy levels of conventional solvents and TTD by density functional theory calculations using the B3LYP/6-311++G** method (Figures 1a and S7). Compared to the relatively high HOMO values of DME (−7.19 eV) and DOL (−7.23 eV), the TTD molecule exhibited a much lower HOMO value of −8.52 eV, even lower than that of EC (−8.47 eV), which is widely used in high-voltage LIBs, thus nicely demonstrating the effect of the molecular level design in tuning the oxidation stability of the

https://doi.org/10.1021/acsaem.2c01261
ACS Appl. Energy Mater. 2022, 5, 7784−7790

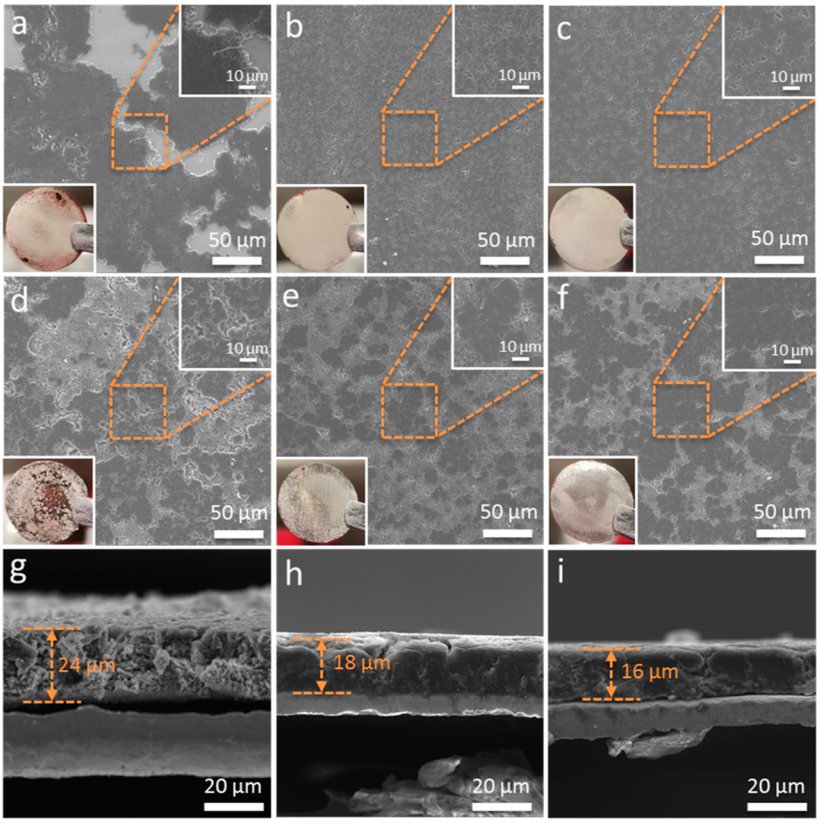

Figure 2. (a–c) SEM analysis of the Li deposition morphology (after the first cycle) in (a) 1 M LiFSI-DME, (b) 1 M LiFSI-8TTD-2DME, and (c) 1.5 M LiFSI-8TTD-2DME electrolytes. (d–f) SEM analysis of the Li deposition morphology after 20 cycles in (d) 1 M LiFSI-DME, (e) 1 M LiFSI-8TTD-2DME, and (f) 1.5 M LiFSI-8TTD-2DME electrolytes. (g–i) SEM analysis (cross-sectional) of plated Li after 20 cycles in (g) 1 M LiFSI-DME, (h) 1 M LiFSI-8TTD-2DME, and (i) 1.5 M LiFSI-8TTD-2DME electrolytes. LilCu half cells were tested at 2 mA cm^{-2} with a cut-off capacity of 2 mA h cm^{-2}. Insets are optical and zoomed-in images.

solvent. In addition, a lower LUMO energy value of TTD (−0.49 eV) could also promote its preferential decomposition on the LMA surface for robust SEI formation. The physical property comparisons of solvents revealed the higher density and boiling point of TTD compared to DME (Table S1). Even though the introduction of $-CF_3$ groups improved the oxidation stability of TTD markedly, it simultaneously reduced its Li-solvation power; hence, the electrolytes were obtained by dissolving 1.5 M or 1 M of the LiFSI salt in TTD and DME in a volume ratio of 8:2 (1 M LiFSI-8TTD-2DME) and 1 M of the LiFSI salt in DME (1 M LiFSI-DME) as a control electrolyte. We observed an increase in both the viscosity (1.2 to 4.9 then 6.7 cP, Table S2) and density of electrolytes (1.074, 1.650, and 1.690 g mL^{-1}) and a reduction in the ionic conductivity (22.5 to 9.4 then 4.7 mS cm^{-1}) going from 1 M LiFSI-DME to 1 M LiFSI-8TTD-2DME and to 1.5 M LiFSI-8TTD-2DME, respectively.

Linear sweep voltammetry (LSV) tests were performed with LilAl cells at a 5 mV s^{-1} scan rate between the open-circuit voltage and 6.5 V to probe the oxidative stability of different electrolytes (Figure 1b). The onset of decomposition started at 4 V in the 1 M LiFSI-DME electrolyte, which is in agreement with the earlier reports in the literature.[21,24] On the contrary, when combined with co-solvent TTD, the electrolyte showed excellent anodic stability of 5.5 V for 1 M LiFSI-8TTD-2DME and 6 V for 1.5 M LiFSI-8TTD-2DME, mainly derived from high-voltage endurance of TTD, and decreased free DME content through the formation of high-concentration DME–Li^+–FSI anion clusters. The oxidation stability of electrolytes was further evaluated in the presence of a conducting agent, Super-P (Figure S8). Cyclic voltammetry (CV) measurements were carried out by using LilCu half cells with the electrolytes to compare the Li deposition/stripping behavior (Figure S9). The overlapping CV curves after the first cycle in the cells with 1 M LiFSI-8TTD-2DME and 1.5 M LiFSI-8TTD-2DME electrolytes revealed a more stable interface formation compared to that of the 1 M LiFSI-DME electrolyte. Moreover, CEs of LilCu half cells with different electrolytes were obtained to assess their stability against LMA. At a current density of 0.5 mA cm^{-2} and a cut-off capacity of 1 mA h cm^{-2}, the CE of 1 M LiFSI-DME exhibited strong fluctuation in 60 cycles, while 1 M LiFSI-8TTD-2DME displayed a stable CE up to 400 cycles, and 1.5 M LiFSI-8TTD-2DME obtained a CE of 99.3% in 570 cycles (Figure S10). Considering the more demanding conditions of practical cells, we further increased the current density and capacity to 2 mA cm^{-2} with 2 mA h cm^{-2} and 3 mA cm^{-2} with 3 mA h cm^{-2}, respectively (Figure 1c,d); the cells containing 1 M LiFSI-DME exhibited fast CE fading in 40 and 25 cycles, while HCE electrolytes such as 4 M LiFSI in a DME solvent (4 M LiFSI-DME), which is known to have good LMA performance through the formation of anion-derived inorganic SEI,[13] could only stabilize up to 85 and 33 cycles (Figures S11 and S12), respectively. In stark contrast, the 1 M LiFSI-8TTD-2DME electrolyte displayed a steady CE over 200 and 110 cycles, and 1.5 M LiFSI-8TTD-2DME showed an excellent CE of 99.3% in 300 cycles and a CE of 99.4% in 210 cycles at 2 mA cm^{-2} with 2 mA h cm^{-2} and 3 mA cm^{-2} with 3 mA h cm^{-2}, respectively. Additionally,

https://doi.org/10.1021/acsaem.2c01261
ACS Appl. Energy Mater. 2022, 5, 7784–7790

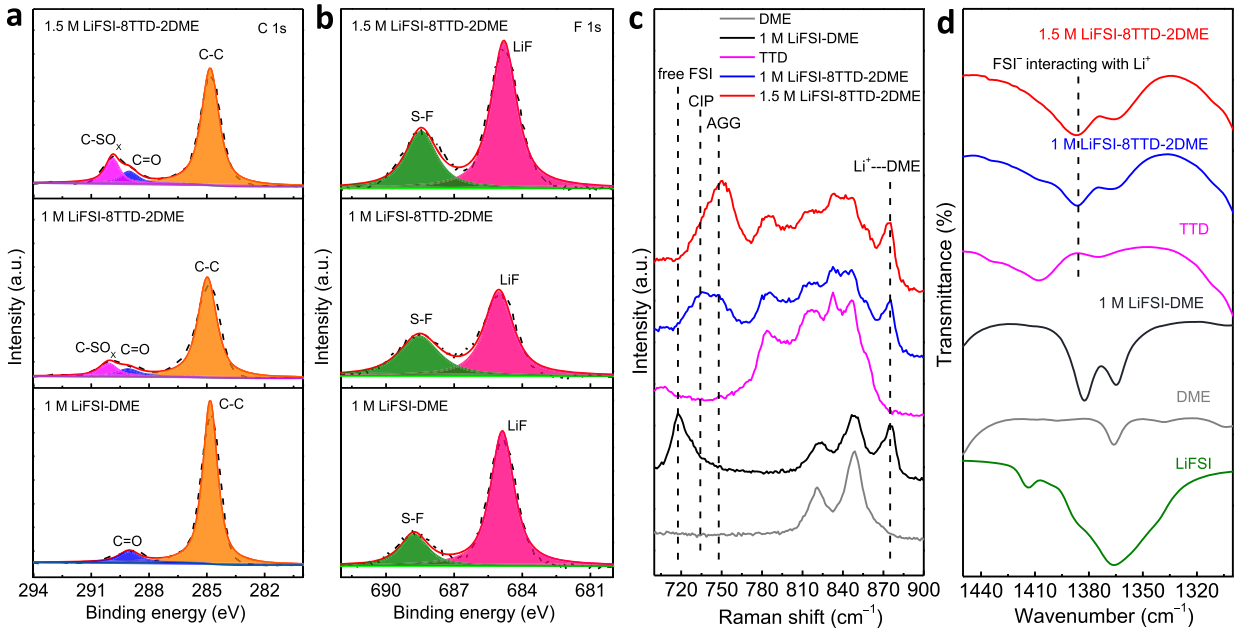

Figure 3. (a,b) C 1s and F 1s XPS profiles of the plated Li surface in Li|Cu half cells with the three electrolytes after 20 cycles at 1 mA cm^{-2}, with a cut-off capacity of 1 mA h cm^{-2}. (c,d) Raman and FTIR spectra of the electrolytes and solvents.

the comparison of CE cycling data of 1 and 1.5 M Li salt revealed the significant impact of salt concentration on stabilizing LMA. Furthermore, the charge−discharge profiles of Li|Cu half cells with different electrolytes were compared at 2 mA cm^{-2} with 2 mA h cm^{-2} capacity (Figure S13). The low stripping capacity in the 1 M LiFSI-DME electrolyte was attributed to the loss and consumption of plated Li after continuous contact with the electrolyte, while a high stripping capacity in both 1 M LiFSI-8TTD-2DME and 1.5 M LiFSI-8TTD-2DME electrolytes revealed reversible Li plating/stripping through the formation of a stable SEI layer on the LMA. A comparison of CE performance with other reports is shown in Table S3. In addition, 1.5 M LiFSI-8DOL-2DME and 1.5 M LiFSI-8EC-2DME were also prepared for comparison in order to clearly demonstrate the impact of molecular engineering in the same volume ratio of 8:2 and by dissolving the 1.5 M LiFSI salt. Li|Cu cells with 1.5 M LiFSI-8DOL-2DME and 1.5 M LiFSI-8EC-2DME electrolytes were evaluated at different capacities and current densities (Figure S14). The CE of cells with 1.5 M LiFSI-8DOL-2DME, which is 98.9%, was found to be stable for 80 cycles at 2 mA cm^{-2} with 2 mA h cm^{-2} and for only 25 cycles at 3 mA cm^{-2} with 3 mA h cm^{-2}, whereas the cells with 1.5 M LiFSI-8EC-2DME displayed continuous fluctuation and fast capacity decay under the same conditions. The carbonate solvent was also evaluated by mixing with TTD at the same volume ratio, which showed inferior performance (Figure S15). In order to investigate interface stability, Li|Li symmetric cells with different electrolytes were cycled at 1 mA cm^{-2} with 1 mA h cm^{-2} capacity. The cells with 1 M LiFSI-8TTD-2DME and 1.5 M LiFSI-8TTD-2DME electrolytes exhibited stable polarization within 300 h; the relatively high polarization values in the range of 35−50 mV were attributed to the moderate ionic conductivity of electrolytes (Figure S16). The Li|Li symmetric cell with 1.5 M LiFSI-8DOL-2DME also showed a stable interface within 200 h, whereas the cell with the 1.5 M LiFSI-8EC-2DME electrolyte showed a large polarization within 10 h, which was followed by a short circuit (Figure S17). Once Al corrosion was investigated with different electrolytes, TTD-based electrolytes exhibited excellent anti-corrosion properties (Figure S18).

Considering the significant impact of electrolytes on Li plating morphology, such as forming filamentous Li dendrites or columnar Li grains,[10] the evolution of plated Li on the Cu substrate, with different electrolytes in Li|Cu half cells during cycling, was evaluated by scanning electron microscopy (SEM) analysis. Li|Cu half cells with different electrolytes were cycled at 2 mA cm^{-2} with a cut-off capacity of 2 mA h cm^{-2}. After the first cycle, plated Li on Cu foil in the 1 M LiFSI-DME electrolyte was uneven and showed Li filaments at the boundary of Li islands along with a bare Cu substrate, which pointed to the growth of an unstable SEI layer and Li-metal consumption through the side reactions with the electrolyte (Figure 2a). On the contrary, the formation of dense and uniform Li grains was shown for both 1 M LiFSI-8TTD-2DME and 1.5 M LiFSI-8TTD-2DME electrolytes with complete coverage on Cu foil (Figure 2b,c). Specifically, larger Li grains were observed at higher salt concentrations, which could further reduce the side reactions with electrolytes derived from the lower surface area, as verified by the cycling results. After 20 cycles, due to the continuous decomposition of the Li salt and solvent, a thick SEI layer and a rough Li surface were observed in the 1 M LiFSI-DME electrolyte along with the exfoliation of dead Li, resulting in the generation of a loose and thick Li anode of 24 μm (Figure 2d,g). In comparison, flat and densely packed Li surfaces with a thickness of 18 μm were obtained in the 1 M LiFSI-8TTD-2DME electrolyte (Figure 2e,h), and an even denser plating occurred in the 1.5 M LiFSI-8TTD-2DME electrolyte owing to the higher salt concentration, enabling larger Li grains, less accumulated SEI, and the lowest thickness of 16 μm (Figure 2f,i) along with a robust SEI layer formation during cycling. The formation of a stable SEI layer and large Li grains is consistent with the excellent electrochemical performance of the TTD-based electrolytes on LMA.

https://doi.org/10.1021/acsaem.2c01261
ACS Appl. Energy Mater. 2022, 5, 7784−7790

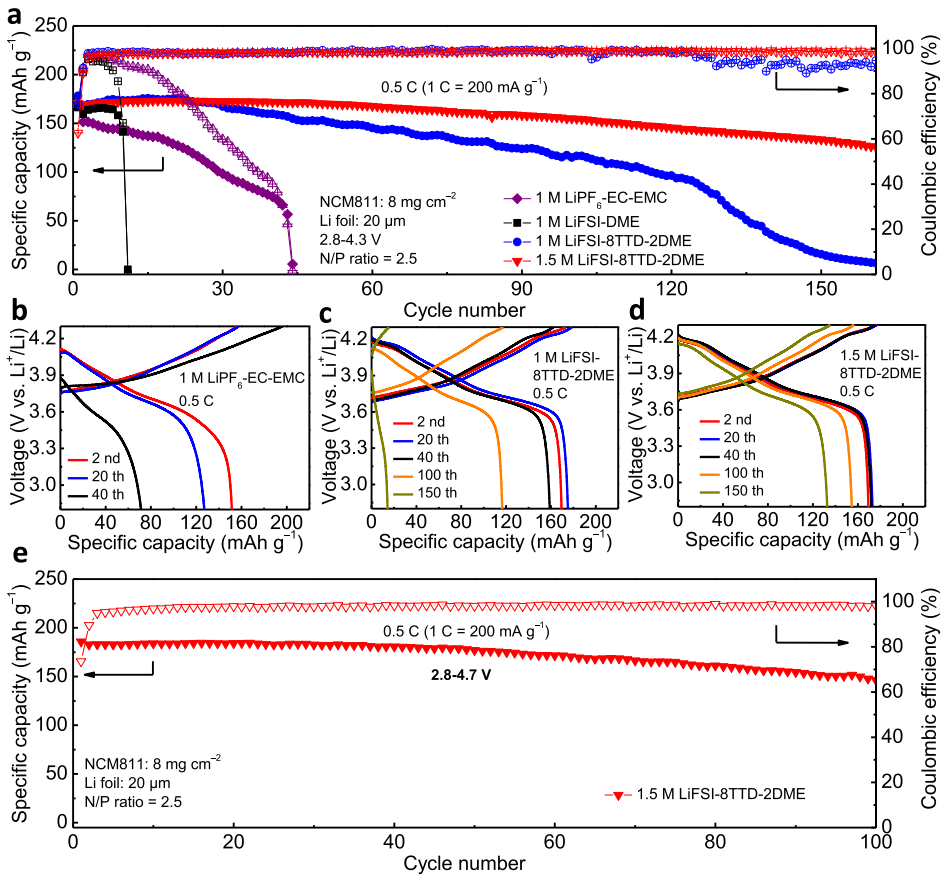

Figure 4. (a) Electrochemical performance of Li|NCM811 full cells at 0.5 C with different electrolytes (after one formation cycle at 0.1 C). (b–d) Charge–discharge profiles of full cells at 0.5 C with (b) 1 M $LiPF_6$-EC-EMC, (c) 1 M LiFSI-8TTD-2DME, and (d) 1.5 M LiFSI-8TTD-2DME electrolytes at different cycles. (e) Cycling performance of Li|NCM811 full cells at 0.5 C with the 1.5 M LiFSI-8TTD-2DME electrolyte (after first formation cycle at 0.1 C) in the high-voltage range of 2.8–4.7 V.

X-ray photoelectron spectroscopy (XPS) measurements were carried out on plated Li in each electrolyte to analyze the SEI composition in Li|Cu half cells after 20 cycles at 1 mA cm^{-2} with a cut-off capacity of 1 mA h cm^{-2} (Figures 3a,b, S19 and S20). In the C 1s spectra, SEI from 1 M LiFSI-DME showed a higher C–C peak intensity (284.8 eV) compared to that of the 1 M LiFSI-8TTD-2DME and 1.5 M LiFSI-8TTD-2DME electrolytes, indicating the formation of an organic-rich SEI layer. The peak at 289.9 eV was assigned to C–SO_x, which originated from FSI anion decomposition[21] and was only observed for the TTD-based electrolytes. In addition, the intensity of this peak further increased upon increasing the concentration of Li salt from 1 to 1.5 M owing to higher anion participation in the SEI growth. Moreover, F 1s spectra revealed higher intensity S–F (688.5 eV) and LiF (685.0 eV) peaks in the 1.5 M LiFSI-8TTD-2DME electrolyte compared to 1 M LiFSI-8TTD-2DME,[21,30] thus proving the formation of the LiF-rich, anion-derived SEI layer and explaining the superior performance of the 1.5 M LiFSI-8TTD-2DME electrolyte in LMA protection. In order to probe the solvation structure of TTD-based electrolytes, Raman spectroscopy analysis was performed (Figure 3c). Compared to the DME solvent, two new peaks at 717 and 875 cm^{-1} in 1 M LiFSI-DME were observed and attributed to the free FSI anion and Li^+ coordinated with the DME solvent, respectively. After adding TTD to replace majority of DME, although the intensities of the free FSI anion and DME peaks significantly decreased, the Li^+–FSI^- association was simultaneously intensified by CIPs (FSI^- coordinating to one Li^+) and aggregate clusters[31] (AGGs, two or more Li^+ coordinating to FSI^-), as evidenced by the emergence of two new peaks at 734 and 748 cm^{-1}, respectively, in 1 M LiFSI-8TTD-2DME electrolyte. When the Li salt concentration increased to 1.5 M, we predominantly observed an AGG peak pointing to the strong association between the FSI anion and multiple Li^+ ions and the absence of free DME or anions.[18] These results explain the excellent anti-oxidation property of 1.5 M LiFSI-8TTD-2DME due to the decreased HOMO level of DME coordinated with Li^+ relative to the FSI anion. In addition, the presence of the AGG cluster also explains the growth of an inorganic SEI layer derived from the FSI anion to realize stable LMA cycling. Fourier-transform infrared (FTIR) spectroscopy analysis was also performed to compare the solvation structure in different electrolytes (Figures 3d and S21). The peaks at 1386 and 1081 cm^{-1} were attributed to coordination of FSI^-–Li^+ and DME–Li^+,[24] which were observed both in 1 M LiFSI-8TTD-2DME and 1.5 M LiFSI-8TTD-2DME and agreed nicely with the Raman results. ^{7}Li NMR spectra of electrolytes also proved the stronger coordination of Li^+ and FSI^- after the introduction of TTD co-solvent (Figure S22).

Considering the advantages of TTD-based electrolytes in terms of oxidation stability and LMA protection, Li|NCM811 full cells with 1 M LiFSI-8TTD-2DME and 1.5 M LiFSI-8TTD-2DME electrolytes were further evaluated. Under the moderate conditions—namely, the Li foil (20 μm) anode paired with the NCM811 cathode (8 mg cm^{-2}) and a

https://doi.org/10.1021/acsaem.2c01261
ACS Appl. Energy Mater. 2022, 5, 7784–7790

negative/positive capacity (N/P) ratio of 2.5—the full cells were cycled at 0.5 C (1 C = 200 mA g^{-1}) with different electrolytes between 2.8 and 4.3 V to probe their feasibility in high-voltage LMBs (Figure 4a). The commercial carbonate electrolyte, that is, 1 M lithium hexafluorophosphate in EC and ethyl methyl carbonate by the volume ratio of 1:1 (1 M $LiPF_6$-EC-EMC) was taken as a reference, which showed fast capacity and CE fading in the Li|NCM811 full cell. There was only 56.6 mA h g^{-1} capacity remaining (37% capacity retention) after 42 cycles originating from Li dendrite formation and serious side reactions on the LMA surface. Owing to its low oxidation stability above 4 V, the full cell performance of 1 M LiFSI-DME was rather poor and was maintained only for nine cycles. In comparison, Li|NCM811 full cells using TTD-based electrolytes showed a marked improvement in both cycling stability and CEs. The full cell with the 1 M LiFSI-8TTD-2DME electrolyte showed 56% capacity retention, 93.8 mA h g^{-1}, after 120 cycles. The full cell with the 1.5 M LiFSI-8TTD-2DME electrolyte, on the other hand, showed the highest capacity of 125.6 mA h g^{-1} after 160 cycles with 75% capacity retention. The difference in the full cell performance between 1 and 1.5 M LiFSI-8TTD-2DME electrolytes was mainly derived from their LMA performance, as also verified by the CE stability tests in Li|Cu half cells. We also compared the charge−discharge profiles of full cells containing different electrolytes (Figures 4b−d and S23). The lower discharge plateau after 40 cycles in 1 M $LiPF_6$-EC-EMC was attributed to the irreversible plating/stripping and thicker SEI formation. The charge profile of 1 M LiFSI-DME at the 10th cycle cannot even reach the cut-off potential owing to the solvent decomposition. The full cells with TTD-based electrolytes, however, showed more stable charge−discharge profiles. Moreover, the full cell with HCE, 4 M LiFSI-DME, was also tested under the same conditions (Figures S24 and S25), which maintained its capacity for only 37 cycles at 0.5 C and showed a charge failure at the 39th cycle. The full cells with 1.5 M LiFSI-8DOL-2DME can operate (Figure S26) for only 10 cycles at 0.5 C due to the continual electrolyte decomposition. The full cell with 1.5 M LiFSI-8EC-2DME showed the worst performance and could not even charge at the first cycle (Figure S27). Electrochemical impedance spectroscopy (EIS) analysis was performed to investigate the interfacial resistance (R_f) in full cells with different electrolytes (Figure S28). After testing at 1 C for 30 cycles, the cell with 1 M $LiPF_6$-EC-EMC exhibited the largest R_f mainly derived from the thick SEI layer formation and porous Li plating by the decomposition of the carbonate solvent. A lower R_f value of 22 Ω was observed in the 1 M LiFSI-DME electrolyte, primarily due to the electrolyte decomposition at a high voltage and unstable SEI layer formation. On the other hand, the full cells with TTD-based electrolytes exhibited the lowest R_f values owing to the presence of an anion-derived, robust SEI layer. We also tested the performance of TTD-based electrolytes under more demanding conditions for practical applications; the NCM811 cathode (high loading of 20 mg cm^{-2}) paired with a 20 μm Li foil with an N/P ratio of 1 was tested with the 1.5 M LiFSI-8TTD-2DME at 0.3 C between 2.8 and 4.4 V, which retained the capacity of 124.8 mA h g^{-1} after 100 cycles with 69% capacity retention (Figure S29). The reproducibility test of three cells under the same conditions revealed consistent cycling stability (Figure S29). In addition, considering the ability of TTD to undergo ring-opening polymerization on the surface of the cathode to form a robust cathode electrolyte interphase, which is not possible with linear or branched diluents/co-solvents, to prevent the dissolution of the transition metals;[32] the Li|NCM811 full cell was cycled at 2.8−4.7 V to realize higher capacity and energy density (Figure 4e), which exhibited 80% capacity retention after 100 cycles at 0.5 C. Electrochemical performance comparison with reported electrolytes is also summarized in Table S4. Compared to the low cut-off voltage of 4.4 V in the reported electrolytes, the TTD-based electrolyte obviously broadened the voltage range of the high-nickel cathode and obtained stable cycling simultaneously.

CONCLUSIONS

We developed a cyclic fluorinated ether as a co-solvent for high-voltage LMBs to overcome the limitations of traditional cyclic solvents such as ethers and carbonates that have low anodic stability and poor compatibility toward the Li metal, respectively. The electrolyte featuring the fluorinated cyclic co-solvent exhibited high oxidative stability up to 6 V and a high CE of 99.4% in 210 cycles under a current density of 3 mA cm^{-2} with 3 mA h cm^{-2} capacity, originating from the strong coordination between Li^+ with DME and the FSI anion and robust SEI formation. The introduction of cyclic TTD also enabled robust cycling of the high-nickel cathode, even up to 4.7 V. These findings open up new avenues for electrolyte engineering toward the realization of high-voltage and practical lithium metal batteries.

ASSOCIATED CONTENT

Supporting Information

The Supporting Information is available free of charge at https://pubs.acs.org/doi/10.1021/acsaem.2c01261.

Experimental section, NMR spectra for all products, electrolyte properties, CE, voltage−time profiles, XPS, FTIR, EIS, and cycling performance (PDF)

AUTHOR INFORMATION

Corresponding Author

Ali Coskun − *Department of Chemistry, University of Fribourg, Fribourg 1700, Switzerland;* orcid.org/0000-0002-4760-1546; Email: ali.coskun@unifr.ch

Authors

Yan Zhao − *Department of Chemistry, University of Fribourg, Fribourg 1700, Switzerland;* orcid.org/0000-0001-5324-5050

Tianhong Zhou − *Department of Chemistry, University of Fribourg, Fribourg 1700, Switzerland;* orcid.org/0000-0002-9537-8465

Mario El Kazzi − *Electrochemistry Laboratory, Paul Scherrer Institute, Villigen 5232, Switzerland;* orcid.org/0000-0003-2975-0481

Complete contact information is available at: https://pubs.acs.org/10.1021/acsaem.2c01261

Author Contributions

Y.Z. and T.Z. contributed equally to this paper. The article was written through contributions of all authors. All authors have approved the final version.

Notes

The authors declare no competing financial interest.

https://doi.org/10.1021/acsaem.2c01261
ACS Appl. Energy Mater. 2022, 5, 7784−7790

■ ACKNOWLEDGMENTS

A.C. acknowledges the support from the Swiss National Science Foundation (SNF) for funding of this research (200021-188572).

■ REFERENCES

(1) Choi, J. W.; Aurbach, D. Promise and reality of post-lithium-ion batteries with high energy densities. *Nat. Rev. Mater.* **2016**, *1*, 16013.
(2) Holoubek, J.; Liu, H.; Wu, Z.; Yin, Y.; Xing, X.; Cai, G.; Yu, S.; Zhou, H.; Pascal, T. A.; Chen, Z.; Liu, P. Tailoring Electrolyte Solvation for Li Metal Batteries Cycled at Ultra-Low Temperature. *Nat. Energy* **2021**, *6*, 303.
(3) Zhang, J.-G.; Xu, W.; Xiao, J.; Cao, X.; Liu, J. Lithium Metal Anodes with Nonaqueous Electrolytes. *Chem. Rev.* **2020**, *120*, 13312−13348.
(4) Lin, D.; Liu, Y.; Cui, Y. Reviving the lithium metal anode for high-energy batteries. *Nat. Nanotechnol.* **2017**, *12*, 194−206.
(5) Kwon, T.-w.; Choi, J. W.; Coskun, A. Prospect for Supramolecular Chemistry in High-Energy-Density Rechargeable Batteries. *Joule* **2019**, *3*, 662−682.
(6) Zheng, X.; Huang, L.; Ye, X.; Zhang, J.; Min, F.; Luo, W.; Huang, Y. Critical effects of electrolyte recipes for Li and Na metal batteries. *Chem* **2021**, *7*, 2312.
(7) Zhang, X.; Yang, Y.; Zhou, Z. Towards practical lithium-metal anodes. *Chem. Soc. Rev.* **2020**, *49*, 3040−3071.
(8) Fang, C.; Li, J.; Zhang, M.; Zhang, Y.; Yang, F.; Lee, J. Z.; Lee, M.-H.; Alvarado, J.; Schroeder, M. A.; Yang, Y.; Lu, B.; Williams, N.; Ceja, M.; Yang, L.; Cai, M.; Gu, J.; Xu, K.; Wang, X.; Meng, Y. S. Quantifying inactive lithium in lithium metal batteries. *Nature* **2019**, *572*, 511−515.
(9) Cheng, X.-B.; Zhang, R.; Zhao, C.-Z.; Zhang, Q. Toward Safe Lithium Metal Anode in Rechargeable Batteries: A Review. *Chem. Rev.* **2017**, *117*, 10403−10473.
(10) Fang, C.; Wang, X.; Meng, Y. S. Key Issues Hindering a Practical Lithium-Metal Anode. *Trends Chem.* **2019**, *1*, 152−158.
(11) Zhou, T.; Zhao, Y.; El Kazzi, M.; Choi, J. W.; Coskun, A. Stable Solid Electrolyte Interphase Formation Induced by Monoquat-Based Anchoring in Lithium Metal Batteries. *ACS Energy Lett.* **2021**, *6*, 1711−1718.
(12) Li, W.; Yao, H.; Yan, K.; Zheng, G.; Liang, Z.; Chiang, Y.-M.; Cui, Y. The synergetic effect of lithium polysulfide and lithium nitrate to prevent lithium dendrite growth. *Nat. Commun.* **2015**, *6*, 7436.
(13) Qian, J.; Henderson, W. A.; Xu, W.; Bhattacharya, P.; Engelhard, M.; Borodin, O.; Zhang, J.-G. High rate and stable cycling of lithium metal anode. *Nat. Commun.* **2015**, *6*, 6362.
(14) Zhao, Q.; Liu, X.; Stalin, S.; Khan, K.; Archer, L. A. Solid-state polymer electrolytes with in-built fast interfacial transport for secondary lithium batteries. *Nat. Energy* **2019**, *4*, 365−373.
(15) Wang, J.; Yamada, Y.; Sodeyama, K.; Chiang, C. H.; Tateyama, Y.; Yamada, A. Superconcentrated electrolytes for a high-voltage lithium-ion battery. *Nat. Commun.* **2016**, *7*, 12032.
(16) Jiao, S.; Ren, X.; Cao, R.; Engelhard, M. H.; Liu, Y.; Hu, D.; Mei, D.; Zheng, J.; Zhao, W.; Li, Q.; Liu, N.; Adams, B. D.; Ma, C.; Liu, J.; Zhang, J.-G.; Xu, W. Stable cycling of high-voltage lithium metal batteries in ether electrolytes. *Nat. Energy* **2018**, *3*, 739−746.
(17) Peng, Z.; Cao, X.; Gao, P.; Jia, H.; Ren, X.; Roy, S.; Li, Z.; Zhu, Y.; Xie, W.; Liu, D.; Li, Q.; Wang, D.; Xu, W.; Zhang, J. G. High-Power Lithium Metal Batteries Enabled by High-Concentration Acetonitrile-Based Electrolytes with Vinylene Carbonate Additive. *Adv. Funct. Mater.* **2020**, *30*, 2001285.
(18) Ren, X.; Gao, P.; Zou, L.; Jiao, S.; Cao, X.; Zhang, X.; Jia, H.; Engelhard, M. H.; Matthews, B. E.; Wu, H.; Lee, H.; Niu, C.; Wang, C.; Arey, B. W.; Xiao, J.; Liu, J.; Zhang, J.-G.; Xu, W. Role of inner solvation sheath within salt-solvent complexes in tailoring electrode/electrolyte interphases for lithium metal batteries. *Proc. Natl. Acad. Sci. U.S.A.* **2020**, *117*, 28603−28613.
(19) Chen, S.; Zheng, J.; Mei, D.; Han, K. S.; Engelhard, M. H.; Zhao, W.; Xu, W.; Liu, J.; Zhang, J. G. High-Voltage Lithium-Metal Batteries Enabled by Localized High-Concentration Electrolytes. *Adv. Mater.* **2018**, *30*, No. e1706102.
(20) Ren, X.; Chen, S.; Lee, H.; Mei, D.; Engelhard, M. H.; Burton, S. D.; Zhao, W.; Zheng, J.; Li, Q.; Ding, M. S.; Schroeder, M.; Alvarado, J.; Xu, K.; Meng, Y. S.; Liu, J.; Zhang, J.-G.; Xu, W. Localized High-Concentration Sulfone Electrolytes for High-Efficiency Lithium-Metal Batteries. *Chem* **2018**, *4*, 1877−1892.
(21) Cao, X.; Ren, X.; Zou, L.; Engelhard, M. H.; Huang, W.; Wang, H.; Matthews, B. E.; Lee, H.; Niu, C.; Arey, B. W.; Cui, Y.; Wang, C.; Xiao, J.; Liu, J.; Xu, W.; Zhang, J.-G. Monolithic solid-electrolyte interphases formed in fluorinated orthoformate-based electrolytes minimize Li depletion and pulverization. *Nat. Energy* **2019**, *4*, 796−805.
(22) Cao, X.; Zou, L.; Matthews, B. E.; Zhang, L.; He, X.; Ren, X.; Engelhard, M. H.; Burton, S. D.; El-Khoury, P. Z.; Lim, H.-S.; Niu, C.; Lee, H.; Wang, C.; Arey, B. W.; Wang, C.; Xiao, J.; Liu, J.; Xu, W.; Zhang, J.-G. Optimization of fluorinated orthoformate based electrolytes for practical high-voltage lithium metal batteries. *Energy Storage Mater.* **2021**, *34*, 76−84.
(23) Cao, X.; Gao, P.; Ren, X.; Zou, L.; Engelhard, M. H.; Matthews, B. E.; Hu, J.; Niu, C.; Liu, D.; Arey, B. W.; Wang, C.; Xiao, J.; Liu, J.; Xu, W.; Zhang, J. G. Effects of fluorinated solvents on electrolyte solvation structures and electrode/electrolyte interphases for lithium metal batteries. *Proc. Natl. Acad. Sci. U.S.A.* **2021**, *118*, No. e2020357118.
(24) Yu, Z.; Wang, H.; Kong, X.; Huang, W.; Tsao, Y.; Mackanic, D. G.; Wang, K.; Wang, X.; Huang, W.; Choudhury, S.; Zheng, Y.; Amanchukwu, C. V.; Hung, S. T.; Ma, Y.; Lomeli, E. G.; Qin, J.; Cui, Y.; Bao, Z. Molecular design for electrolyte solvents enabling energy-dense and long-cycling lithium metal batteries. *Nat. Energy* **2020**, *5*, 526−533.
(25) Xue, W.; Huang, M.; Li, Y.; Zhu, Y. G.; Gao, R.; Xiao, X.; Zhang, W.; Li, S.; Xu, G.; Yu, Y.; Li, P.; Lopez, J.; Yu, D.; Dong, Y.; Fan, W.; Shi, Z.; Xiong, R.; Sun, C.-J.; Hwang, I.; Lee, W.-K.; Shao-Horn, Y.; Johnson, J. A.; Li, J. Ultra-high-voltage Ni-rich layered cathodes in practical Li metal batteries enabled by a sulfonamide-based electrolyte. *Nat. Energy* **2021**, *6*, 495−505.
(26) Aurbach, D.; Youngman, O.; Gofer, Y.; Meitav, A. The electrochemical behaviour of 1,3-dioxolane-LiClO4 solutions-I. Uncontaminated solutions. *Electrochim. Acta* **1990**, *35*, 625−638.
(27) Aurbach, D. Review of selected electrode-solution interactions which determine the performance of Li and Li ion batteries. *J. Power Sources* **2000**, *89*, 206−218.
(28) Liu, F. Q.; Wang, W. P.; Yin, Y. X.; Zhang, S. F.; Shi, J. L.; Wang, L.; Zhang, X. D.; Zheng, Y.; Zhou, J. J.; Li, L.; Guo, Y. G. Upgrading traditional liquid electrolyte via in situ gelation for future lithium metal batteries. *Sci. Adv.* **2018**, *4*, No. eaat5383.
(29) Li, T.; Zhang, X.-Q.; Shi, P.; Zhang, Q. Fluorinated solid-electrolyte interphase in high-voltage lithium metal batteries. *Joule* **2019**, *3*, 2647−2661.
(30) Miao, R.; Yang, J.; Xu, Z.; Wang, J.; Nuli, Y.; Sun, L. A new ether-based electrolyte for dendrite-free lithium-metal based rechargeable batteries. *Sci. Rep.* **2016**, *6*, 21771.
(31) Yamada, Y.; Yaegashi, M.; Abe, T.; Yamada, A. A superconcentrated ether electrolyte for fast-charging Li-ion batteries. *Chem. Commun.* **2013**, *49*, 11194−11196.
(32) Zheng, Q.; Yamada, Y.; Shang, R.; Ko, S.; Lee, Y.-Y.; Kim, K.; Nakamura, E.; Yamada, A. A cyclic phosphate-based battery electrolyte for high voltage and safe operation. *Nat. Energy* **2020**, *5*, 291−298.

https://doi.org/10.1021/acsaem.2c01261
ACS Appl. Energy Mater. 2022, 5, 7784−7790